This article has been accepted for publication in a future issue of this journal, but has not been fully edited. Content may change prior to final publication. Citation information: DOI 10.1109/TPEL.2016.2621064, IEEE Transactions on Power Electronics

Unified Wide-Speed Sensorless Scheme Using Nonlinear Optimization for IPMSM Drives

Yingguang Sun, *Student Member, IEEE,* Matthias Preindl, *Member, IEEE,* Shahin Sirouspour, *Member, IEEE,* and Ali Emadi, *Fellow, IEEE*

***Abstract*—This paper proposes a novel unified nonlinear optimization based speed and position estimation algorithm for Interior Permanent Magnet Synchronous Motor (IPMSM) drives at wide speed range operations. A cost function based on the voltage equations in the stationary reference frame is employed for speed and position estimation. The speed and position can be estimated by minimizing the cost function. At low speed including standstill condition, the cost function is modified and high frequency sinusoidal voltage signals are injected in the estimated magnetic axis. A Phase Locked Loop (PLL) is combined with the proposed position estimator for reducing the noise of estimation results. Compared with existing sensorless methods, a unified estimator is used at low and high speed operations and a better performance is obtained in transient and steady state conditions. The convexity of the cost functions with respect to the speed and position estimation errors is analyzed in the paper. The feasibility of the proposed estimation algorithm is validated with an experimental test bench.**

***Index Terms*—Interior permanent magnet synchronous motor drives, motor control, nonlinear optimization, position sensorless.**

I. Introduction

PERMANENT magnet synchronous machines (PMSM) are known for their high power density, high efficiency, simple structure and ease of control. High performance of PMSM drives requires the knowledge of speed and rotor position for vector control. Position sensors (resolver and encoder) have several drawbacks such as increased motor size, decreased robustness and reliability of drive system and additional cost. Hence, motor control research has been focused on replacing position sensors with observers and estimators that avoid sensor-related issues [1].

Sensorless control methods can be classified into two categories. The first category is electromotive force (EMF) based estimation methods relying on measurement of stator voltages and currents for medium and high speed operations [2]–[18]. The most straightforward way of obtaining the position information is to calculate the EMF or flux in open loop or simply estimating flux by integrating the EMF. However, the integration degrades due to the drift problem and is sensitive to machine phase resistance. In order to improve position estimation, the EMF, extended EMF and flux were estimated by state observers [2]–[9], sliding mode observers [10]–[15] and extended Kalman Filters [16]–[18]. Since the EMF components are proportional to the motor speed, the extraction of EMF is challenging at low speed condition. Moreover, the voltage drop due to the stator resistance and inverter nonlinearities also affect estimation performance of the EMF based methods at low speed.

In order to improve speed and position estimation at low speed, the saliency tracking based methods, which usually employ high frequency signal injection into different frames of the machine [19]–[31], are also widely utilized. These methods exploited the anisotropic property of the permanent magnet machine caused by spatial saliency or magnetic saturation. In [19]–[22], rotating sinusoidal voltage signals were injected into stationary reference frame and the resulting carrier frequency currents were demodulated for extracting the rotor position information. Another major type of injection method is called pulsating voltage injection method [23]–[26]. This method relied on injecting sinusoidal voltage signals into the estimated d or q axis and the induced currents in the estimated q or d axis was utilized for position estimation. Other types of injection like square wave voltage injection [27]–[29], sinusoidal current injection [30] and pulsating voltage injection into stationary reference frame [31] were also applied for position sensing in PMSM drives. The saliency tracking based methods are parameter independent and suitable for low speed operations including standstill conditions. However, larger torque ripples and extra losses are introduced by these methods due to the superimposition of extra signals on the fundamental frequency components. Additionally, the control bandwidth is limited due to demodulation of the carrier frequency current components in position estimation. Besides signal injection, methods relying on high frequency excitation by PWM switching [32], [33] were also employed for sensorless control of PMSM drives.

Combination of EMF based methods and saliency tracking based methods is a widely employed solution for applying sensorless control algorithms on PMSM drives at wide speed range operation. At low speed, the saliency tracking based methods are employed. The EMF based estimation methods take over at medium and high speed conditions. During the transition between low speed and medium speed, several combination algorithms were proposed. In [34]–[36], variable observer structures or gains were applied at different

This paper has not been published in any conference proceedings or journals.

Yingguang Sun and Ali Emadi are with the McMaster Automotive Resource Centre (MARC), McMaster University, Hamilton, Ontario, L8P 0A6, Canada (email: suny77@mcmaster.ca; emadi@mcmaster.ca).

Matthias Preindl is with the Electrical Engineering Department, Columbia University in the City of New York, NY, 10027, United States (email: matthias.preindl@columbia.edu).

Shahin Sirouspour is with the Department of Electrical and Computer Engineering, McMaster University, Hamilton, Ontario, LS4 4K1, Canada (email:sirous@mcmaster.ca).

This article has been accepted for publication in a future issue of this journal, but has not been fully edited. Content may change prior to final publication. Citation information: DOI 10.1109/TPEL.2016.2621064, IEEE Transactions on Power Electronics

speed ranges. In [37]–[39], a linear blending combination was proposed between EMF based methods and saliency tracking based methods during the switching process. However, involving two independent position estimators with different structures increases system complexity and decreases system robustness.

This paper proposes a nonlinear optimization based position and speed estimation algorithm for wide speed range operations. A cost function based on voltage equations in the stationary reference frame is employed for speed and position estimation. The speed and position are both involved in the cost function and they are decision variables for this nonlinear optimization problem. The speed and position can be estimated by minimizing the proposed cost function based on measurements of stator voltages and currents. Since the voltage information is less significant at low speed and unable to be observed at standstill condition, extra high frequency sinusoidal voltages are injected in estimated magnetic axis. Extra regularization terms are added in the cost function at low speed to improve estimation quality. A Phase Locked Loop (PLL) is involved at the output of the position estimator serving as a filter. In this way, a unified position and speed estimation method is proposed for wide speed range operation without switching between different position estimation algorithms. The system block diagram is shown in Fig. 1. Convexity analysis on the cost function under different speeds and positions are also illustrated in this paper. The feasibility of the proposed estimation algorithm is validated with the prototype interior permanent magnet (IPM) motor drive system under different experimental testing conditions.

The rest of this paper is organized as follows. Section II introduces the optimization based sensorless algorithm. Section III presents the observer implementation. Section IV is concerned with experimental results of the proposed method. The paper is concluded in Section V.

II. Optimization Based Sensorless Algorithm

Three reference frames in sensorless permanent magnet motor drives are shown in Fig. 2. The voltages and currents in the stationary reference frame (α-β frame) can be transformed into rotor reference frame (d-q frame) or estimated rotor reference frame (δ-γ frame) by actual position θ or estimated position $\hat{\theta}$.

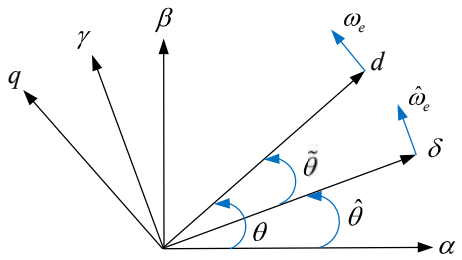

Fig. 2. Different reference frames in sensorless PMSM drives.

The discrete voltage equations of IPM motor in the rotor reference frame are

$$\begin{bmatrix}\bar{u}_d(k)\\ \bar{u}_q(k)\end{bmatrix} = \frac{1}{T_s}\begin{bmatrix}L_d & 0\\ 0 & L_q\end{bmatrix}\left(\begin{bmatrix}i_d(k+1)\\ i_q(k+1)\end{bmatrix} - \begin{bmatrix}i_d(k)\\ i_q(k)\end{bmatrix}\right) - \omega_e(k)\left(\begin{bmatrix}0 & L_q\\ -L_d & 0\end{bmatrix}\begin{bmatrix}i_d(k)\\ i_q(k)\end{bmatrix} - \begin{bmatrix}0\\ \lambda_{pm}\end{bmatrix}\right). \quad (1)$$

The i_{dq} and L_{dq} denote the currents and inductances in d-q frame. The $\omega_e(k)$, λ_{pm} and T_s represent the electrical speed, permanent magnet flux linkage and sampling time respectively. The compensated voltage in d-q frame can be calculated by $\bar{u}_{dq} = u_{dq} - R_s i_{dq}$ [40], where R_s denotes the machine phase resistance.

If (1) is transformed into α-β frame by actual position $\theta(k)$, then the equations are written in (2).

The $\bar{u}_{\alpha\beta}$ and $i_{\alpha\beta}$ represent the compensated voltages and the currents in α-β frame. The position difference between two consecutive sample times is calculated as $\Delta\theta(k) = T_s\omega_e(k)$. The transformation T_{pk} then is represented in

$$T_{pk}\big(\Delta\theta(k)\big) = \begin{bmatrix}\cos\big(\Delta\theta(k)\big) & \sin\big(\Delta\theta(k)\big)\\ -\sin\big(\Delta\theta(k)\big) & \cos\big(\Delta\theta(k)\big)\end{bmatrix}. \quad (3)$$

The position dependent matrices $L_{ab}\big(\theta(k)\big)$ are calculated as

$$L_a\big(\theta(k)\big) = \begin{bmatrix}L_1 + L_2\cos 2\theta(k) & L_2\sin 2\theta(k)\\ L_2\sin 2\theta(k) & L_1 - L_2\cos 2\theta(k)\end{bmatrix} \quad (4)$$

$$L_b\big(\theta(k)\big) = \begin{bmatrix}L_2\sin 2\theta(k) & L_1 - L_2\cos 2\theta(k)\\ -L_1 - L_2\cos 2\theta(k) & -L_2\sin 2\theta(k)\end{bmatrix}, \quad (5)$$

where $L_1 = (L_d + L_q)/2$ and $L_2 = (L_d - L_q)/2$.

If the terminal quantities in α-β frame and the motor parameters are known, the speed and position can be extracted by solving the nonlinear equations in (2). If a cost function is defined in (6) based on (2), then the cost is zero if actual position and speed are used. Since only estimated position and speed exist in the sensorless control system, the cost will be zero if the estimated speed and position are exactly the actual ones.

Fig. 3 shows the contour plots of the cost function at different speed and current conditions. The horizontal axis is the position estimation error and the vertical axis is the speed estimation error. From the contour plots, it is clear that the cost decreases as the estimated speed and position approach to the actual speed and position. The cost function has two local minimums in one electrical period. If the machine is running at N rpm, the first local minimum locates at the origin. The speed and position errors are both zero, which indicates the correct estimation. The second local minimum's coordinate is (180°, -2N rpm) which corresponds to the negative direction of the magnetic axis. Therefore, the speed and position estimation becomes an online nonlinear optimization problem with two decision variables and the estimation can be achieved by minimizing the cost function (6).

If the cost function is locally convex and if the initial values of each estimation are around the expected local minimum, the optimization is able to reach the expected local minimum with finite iterations. A function is said to be convex if its second derivative (Hessian) is positive semi-definite in a convex set [41]. However, the analytical demonstration is challenging due

This article has been accepted for publication in a future issue of this journal, but has not been fully edited. Content may change prior to final publication. Citation information: DOI 10.1109/TPEL.2016.2621064, IEEE Transactions on Power Electronics

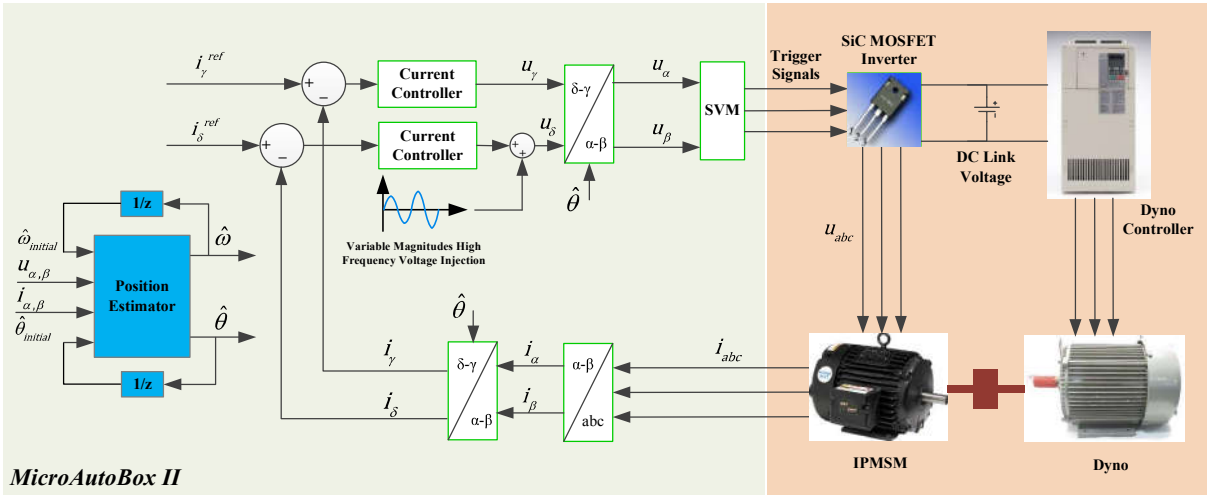

Fig. 1. Block diagram of proposed IPMSM sensorless drives.

$$\begin{bmatrix}\bar{u}_\alpha(k)\\ \bar{u}_\beta(k)\end{bmatrix} - \frac{L_a\big(\theta(k)\big)}{T_s}\left(T_{pk}\big(\Delta\theta(k)\big)\begin{bmatrix}i_\alpha(k+1)\\ i_\beta(k+1)\end{bmatrix} - \begin{bmatrix}i_\alpha(k)\\ i_\beta(k)\end{bmatrix}\right) + \omega_e(k)\left(L_b\big(\theta(k)\big)\begin{bmatrix}i_\alpha(k)\\ i_\beta(k)\end{bmatrix} + \lambda_{pm}\begin{bmatrix}\sin\theta(k)\\ -\cos\theta(k)\end{bmatrix}\right) = 0. \tag{2}$$

$$\begin{aligned}\underset{\hat{\theta}(k),\hat{\omega}(k)}{\text{minimize}} \quad G\left(\hat{\theta}(k),\hat{\omega}_e(k)\right) = \Bigg\| &\bar{u}_{\alpha\beta}(k) - \frac{L_a\big(\hat{\theta}(k)\big)}{T_s}\Big(T_{pk}\big(\Delta\hat{\theta}(k)\big)i_{\alpha\beta}(k+1) - i_{\alpha\beta}(k)\Big)\\ &+ \hat{\omega}_e(k)\left(L_b\big(\hat{\theta}(k)\big)i_{\alpha\beta}(k) + \lambda_{pm}\begin{bmatrix}\sin\hat{\theta}(k)\\ -\cos\hat{\theta}(k)\end{bmatrix}\right)\Bigg\|^2\end{aligned} \tag{6}$$

to the complexity of the Hessian of the proposed cost function. A real symmetric matrix is said to be positive semi-definite if all its eigenvalues are non-negative. In the proposed cost function, the Hessian is a 2×2 real symmetric matrix and has two eigenvalues. The local convexity of the cost function around the two local minimums is illustrated by plotting the region in which both the eigenvalues of the Hessian are non-negative. The procedures are: (a) The eigenvalues of the Hessian are calculated at different speeds and positions with 0.4° degree and 10 rpm intervals; (b) If the two eigenvalues are both non-negative, the point is recorded and plotted on the contour plot of the cost function; (c) The convex regions are then depicted in Fig. 4 and Fig. 5. The plots were also depicted with speed and position intervals as small as 0.1° degree and 1 rpm. The convex regions with smaller intervals have the same envelops with Fig. 4 and Fig. 5 but with more points included. The idea of illustrating the observer convergence with plots or system trajectories has already been used in [4], [42]. In Fig. 4 (b) and Fig. 5 (b), the zoomed in convex regions around the expected local minimum are shown. The convergence of the proposed estimator is guaranteed if the speed and position errors are within those regions. Outside these regions, no convergence guarantees can be issued.

Since the back-emf is proportional to the machine speed, the voltage magnitudes in (6) are more significant at higher speed. The size of the local convex region increases at higher speed due to the increase of voltages, as illustrated in Fig. 4 and Fig. 5. At very low speed including standstill condition, (6) is not convex in Fig. 6 (a) and Fig. 7 (a). In order to estimate the speed and position at low speed, high frequency sinusoidal voltages are injected in δ axis and (6) is modified in

$$\begin{aligned}&\underset{\hat{\theta}(k),\hat{\omega}(k)}{\text{minimize}} \quad G_l(\hat{\theta}(k),\hat{\omega}_e(k)) = G\left(\hat{\theta}(k),\hat{\omega}_e(k)\right)\\ &+ K_1\left(\hat{\theta}(k) - \hat{\theta}(k-1)\right)^2 + K_2\left(\hat{\omega}_e(k) - \hat{\omega}_e(k-1)\right)^2.\end{aligned} \tag{7}$$

The extra regularization terms $K_1\left(\hat{\theta}(k) - \hat{\theta}(k-1)\right)^2$ and $K_2\left(\hat{\omega}_e(k) - \hat{\omega}_e(k-1)\right)^2$ are added in the cost function as a filter. Improvements of the cost function can be found in the comparisons between Fig. 6 (a), (b) and Fig. 7 (a), (b). The $\hat{\omega}_e(k-1)$ and $\hat{\theta}(k-1)$ are assumed to be actual speed and position in Fig. 6 (b) and Fig. 7 (b). With modification of the cost function and involvement of the voltage injection, the plot of the cost function (7) become convex and has only one minimum at origin in one electrical period. The convex regions of the modified cost function at 0 rpm and 50 rpm are shown in Fig. 8. The K_1 and K_2 are both set to zero at high speed conditions.

This article has been accepted for publication in a future issue of this journal, but has not been fully edited. Content may change prior to final publication. Citation information: DOI 10.1109/TPEL.2016.2621064, IEEE Transactions on Power Electronics

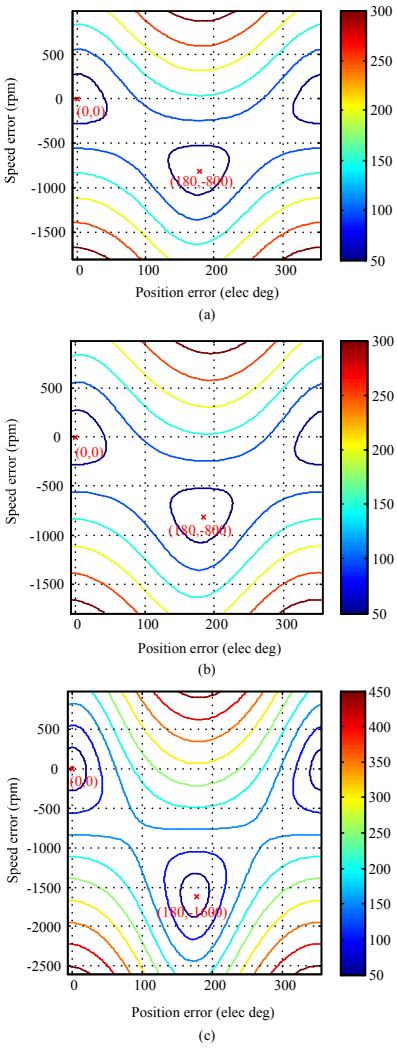

Fig. 3. Contour plots of the cost function (6): (a) 400 rpm and $i_{phase}^{peak} = 0$; (b) 400 rpm and $i_{phase}^{peak} = 4$; (c) 800 rpm and $i_{phase}^{peak} = 0$.

III. Observer Implementation

In the real time implementation, Newton's method is employed for minimizing the cost functions shown in (6) and (7) numerically. The compensated voltages $\overline{u}_{\alpha\beta}$ and the measured currents $i_{\alpha\beta}$ are employed for estimation at the sampling frequency. First of all, estimated speed and position in the previous sample time are set as the initial values for the optimization. Then the decent direction is computed by calculating the partial derivatives J (2×1 matrix) and Hessian matrix H of the cost function. The coefficient ξ is searched for minimizing the cost by using the line search method. At the end of each estimation, the new decision variables $\hat{\theta}(k+1)$ and $\hat{\omega}(k+1)$ are updated with

$$\begin{bmatrix} \hat{\theta}(k+1) \\ \hat{\omega}(k+1) \end{bmatrix} = \begin{bmatrix} \hat{\theta}(k) \\ \hat{\omega}(k) \end{bmatrix} - \xi H^{-1} J. \tag{8}$$

The newly updated $\hat{\theta}(k+1)$ and $\hat{\omega}(k+1)$ are utilized as initial values for the next estimation. The proposed optimization based estimator is depicted in the left side of Fig. 9. Since the estimator issues a position and speed estimation based on

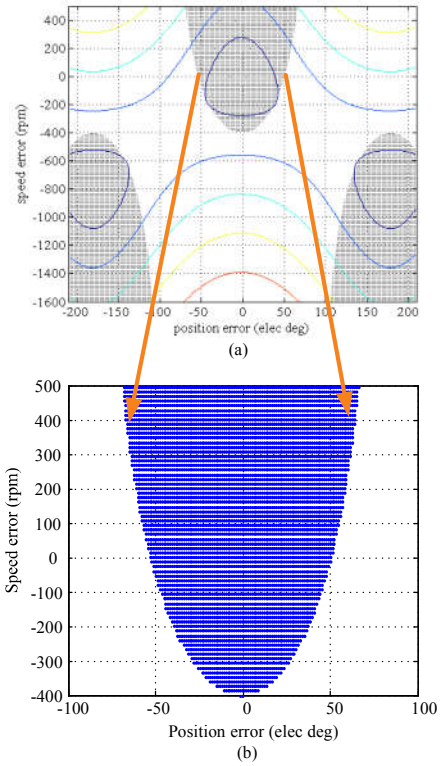

Fig. 4. Convex region of the cost function (6) at 400 rpm: (a) convex regions on the contour plot; (b) zoomed in convex region around the expected local minimum.

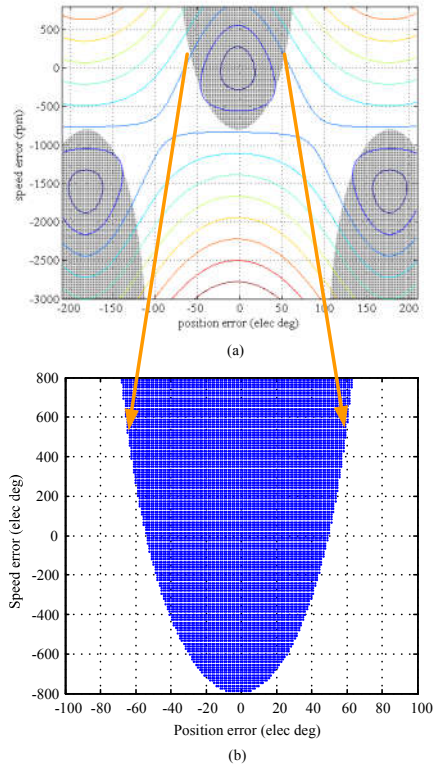

Fig. 5. Convex region of the cost function (6) at 800 rpm: (a) convex regions on the contour plot; (b) zoomed in convex region around the expected local minimum.

This article has been accepted for publication in a future issue of this journal, but has not been fully edited. Content may change prior to final publication. Citation information: DOI 10.1109/TPEL.2016.2621064, IEEE Transactions on Power Electronics

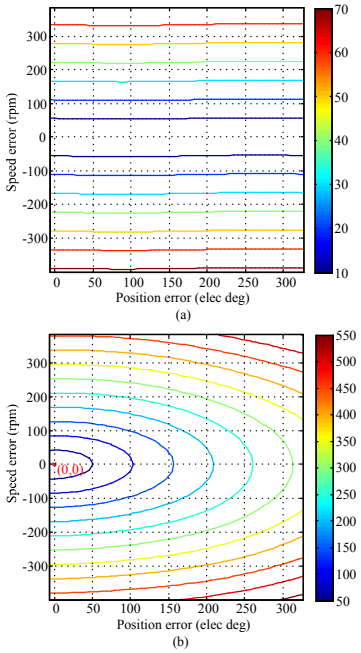

Fig. 6. Contour plots of the cost function: (a) cost function (6) at 0 rpm without injection; (b) cost function (7) at 0 rpm with injection.

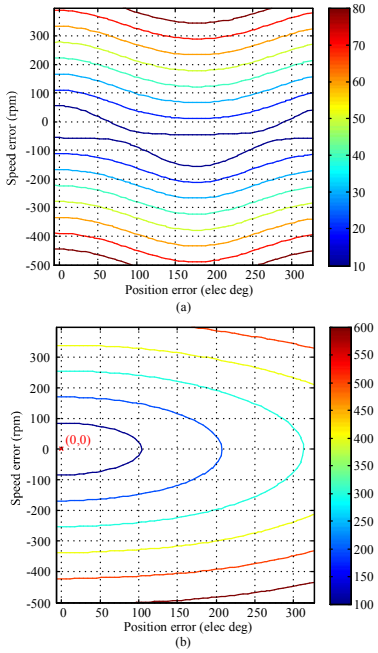

Fig. 7. Contour plots of the cost function: (a) cost function (6) at 50 rpm without injection; (b) cost function (7) at 50 rpm with injection.

instantaneous values, current sensor noises directly affect the estimation quality. In order to filter high frequency noises, a Phase Locked Loop (PLL) is implemented in series with the proposed estimator, as shown in the right side of Fig. 9. The PLL consists of a PI regulator, a discrete integrator, a speed feed-forward term and a digital filter. The filtered estimated speed and position are utilized for motor control.

In the unified sensorless control algorithm, a variable magnitudes high frequency voltage injection method is employed at low speed. The high frequency sinusoidal voltage is injected in δ axis and superimposed on the fundamental frequency

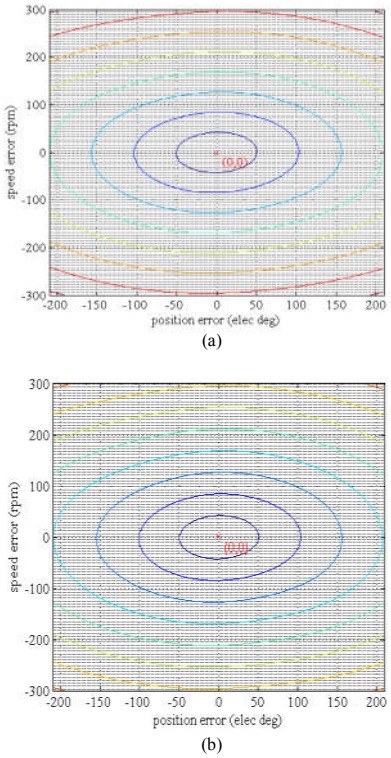

Fig. 8. Convex regions of the modified cost function: (a) convex region at 0 rpm; (b) convex region at 50 rpm.

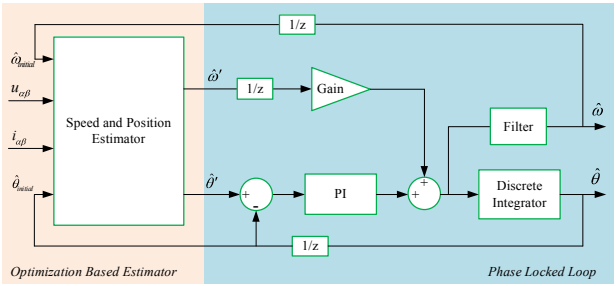

Fig. 9. Proposed nonlinear optimization based position estimator.

voltages. The injection scheme is shown in

$$V_{inj} = \begin{cases} \frac{N_1 - |\hat{N}|}{N_1} V_1 & |\hat{N}| \le N_1 \\ 0 & |\hat{N}| > N_1 \end{cases} \quad (9)$$

as well as Fig. 10. The $\hat{N}$ denotes the estimated speed in rpm. In this way, the injected voltage is adjusted according to the estimated speed and extra loss is reduced. In summary, the original cost function (6) is utilized for estimation without injection when the motor speed is higher than N_1. The variable magnitudes high frequency voltage injection and the modified cost function (7) are employed when the motor speed is lower than N_1. The K_1 and K_2 were tuned heuristically in simulation and experiments. In the proposed PLL, the speed feed-forward term is used for accelerating the dynamic response and the digital filter is employed for speed ripple reduction. The proportional and integral gains in the PI regulator can be designed based on the PLL bandwidth requirements, but

This article has been accepted for publication in a future issue of this journal, but has not been fully edited. Content may change prior to final publication. Citation information: DOI 10.1109/TPEL.2016.2621064, IEEE Transactions on Power Electronics

the theoretical numbers need to be adjusted by balancing the estimation bandwidth and noise attenuation [20], [24], [43] in experimental tests. The switch from (7) to (6) is achieved by setting K_1 and K_2 to zero. The algorithm for speed and position estimation at low speed and high speed is unified instead of combining different estimation methods in [34]–[39].

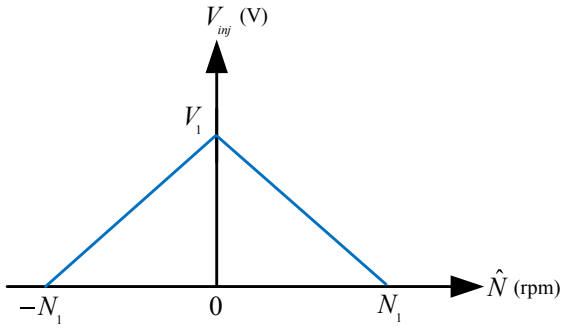

Fig. 10. Variable magnitudes voltage injection scheme.

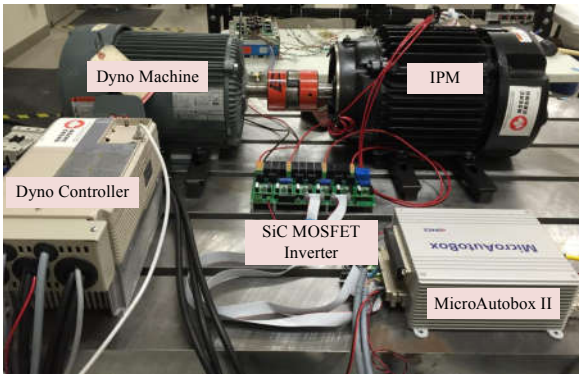

Fig. 11. Prototype IPM motor drives test bench.

IV. Experimental Verification

A. Experimental Prototype

The proposed unified speed and position estimation algorithm was tested in the experimental test bench shown in Fig. 11. Table I lists the parameters of the prototype IPM motor drive system. The switching frequency and sampling frequency were both set to 10 kHz. The DC linkage voltage was 300 V. Speed control was implemented in the dyno machine and the IPM motor was under torque control. The i_δ was controlled to be zero and the i_γ was controlled for electromagnetic torque generation. The injection voltage magnitude V_1 was 70 V and the speed N_1 was set to 400 rpm. The frequency of the injected sinusoidal voltage was 500 Hz.

In Fig. 8, the cost function becomes convex if the estimated speed and position in the previous sampling time are used in the modified cost function (7). Hence, the initial rotor position needs to be detected as the initial value at the machine start-up. In this paper, the initial position was estimated by the methods mentioned in [1]. Since this paper is mainly focus on the speed and position estimation at running state, all the results are under the assumption that the initial position has already been known.

TABLE I
Parameters of IPMSM and Drive Used in Experiment

Parameter	Value
Number of pole pairs P	5
Rated current I_r	9.4 A
Rated torque T_r	29.7 Nm
d axis inductance L_d	10.5 mH
q axis inductance L_q	12.9 mH
Stator resistance R_s	400 $m\Omega$
PM flux λ_{pm}	343.05mWb
DC link voltage U_{dc}	300 V
Sampling time T_s	100 μs

The position estimation error $\tilde{\theta} = \theta - \hat{\theta}$ may increase during the speed or torque transients. The inaccurate initial position estimation method may also lead to a large position estimation error. The robustness of position estimators is reflected in the capability of converging to the correct estimation from a certain initial estimation error. Fig. 12 shows the convergence range of the proposed position estimator at standstill condition. With $\pm 86°$ initial error, the 10%-90% rise time t_r of the estimator is 0.028 s for both conditions. The practical bandwidth f_{bw} [44] can be calculated in

$$f_{bw} = \frac{0.34}{t_r}, \tag{10}$$

which is 12.14 Hz.

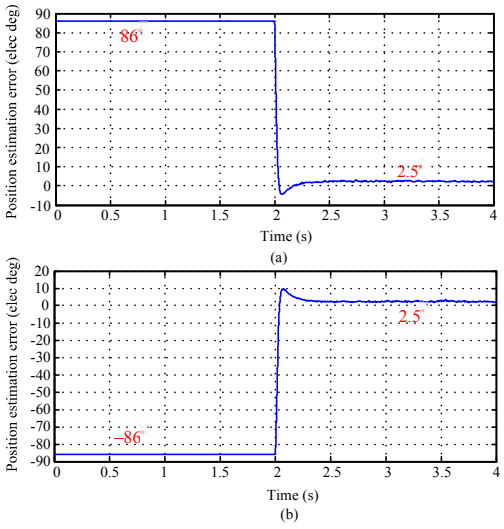

Fig. 12. Experimental results, convergence tests at standstill condition: (a) positive initial error; (b) negative initial error.

Fig. 13 shows the speed and position estimations before and after PLL. Fig. 13 (a) depicts the position estimation when the speed changed from 100 rpm to -100 rpm. From this figure, it is concluded that the speed and position are able to be estimated by the optimization based estimator without PLL. However, involvement of PLL reduces the noises especially in the position estimation and improves the estimation quality.

This article has been accepted for publication in a future issue of this journal, but has not been fully edited. Content may change prior to final publication. Citation information: DOI 10.1109/TPEL.2016.2621064, IEEE Transactions on Power Electronics

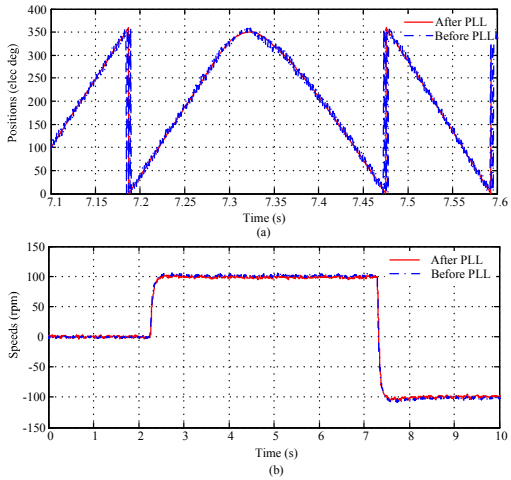

Fig. 13. Experimental results, speed and position estimation before and after PLL: (a) position estimation at transients; (b) speed estimation.

B. Speed Transients Performance

In this section, the estimation performances of the proposed estimator are tested when different speed steps are applied by the dyno motor. Fig. 14 depicts the speed and position estimation with a 50 rpm speed step change. The motor was at standstill condition and then the speed reference increased to 50 rpm and then changed to -50 rpm. Fig. 14 (a), (b) and (c) illustrate the position estimation error, the position estimation at speed transients and the speed estimation respectively. Without extra load torque, the steady state position estimation error is within 3° in electrical degree.

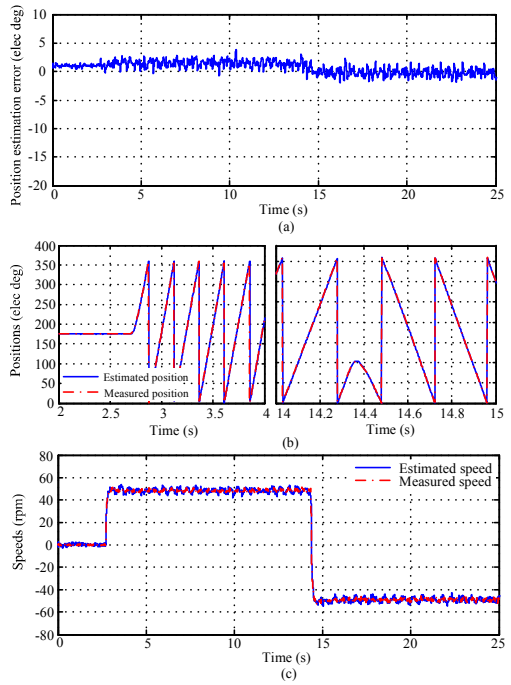

Fig. 14. Experimental results, speed step change without load, 50 rpm: (a) position estimation error; (b) position estimation at transients; (c) speed estimation.

The test in Fig. 14 was repeated with 20% and 40% rated torque applied by the IPM motor respectively. As shown in Fig. 15 (a) and Fig. 16 (a), the maximum steady state estimation errors increase to $-5°$ with 20% rated torque and $-10°$ with 40% rated torque. At low speed, the proposed position estimator relies more on the position information contained in $L_a\big(\theta(k)\big)$, which employs constant inductance values. When the torque related γ axis current are increased in Fig. 15 and Fig. 16, the position estimation errors increase due to the cross-saturation effect [45]. This torque related error can be compensated by involving a current dependent correction term mentioned in [46].

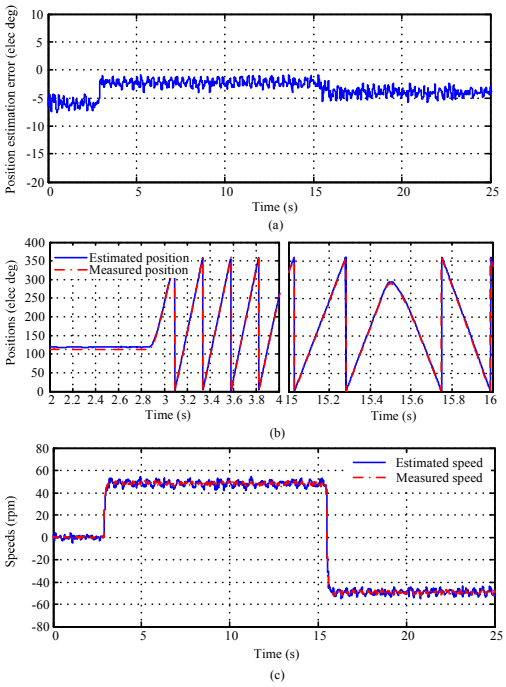

Fig. 15. Experimental results, speed step change with 20% rated torque, 50 rpm: (a) position estimation error; (b) position estimation at transients; (c) speed estimation.

In order to benchmark the propose method, the widely used pulsating voltage injection method [23]–[26] was implemented on the prototype machine drive system as well. In this method, the high frequency sinusoidal voltage is also injected in δ axis and the γ axis current is demodulated for extracting the speed and position information. Fig. 17 depicts the block diagram of the demodulation based position estimator used in the benchmark pulsating sinusoidal voltage injection method. The bandwidth of the PLL used in the demodulation based estimator was tuned to be 36 times larger than that of the PLL used in the proposed position estimator, in order to achieve similar bandwidths with the proposed method in speed and current responses. In the proposed method, the voltage used for the speed and position estimation is the superimposition of both the injected high frequency voltage and the fundamental frequency voltage. However, the position estimation solely relies on the injection frequency voltage in the benchmark reference method. Hence, the magnitude of the injected voltage is kept constant at 70V in the benchmark reference method.

The test shown in Fig. 16 was duplicated with benchmark reference method and the results are shown in Fig. 18. As

This article has been accepted for publication in a future issue of this journal, but has not been fully edited. Content may change prior to final publication. Citation information: DOI 10.1109/TPEL.2016.2621064, IEEE Transactions on Power Electronics

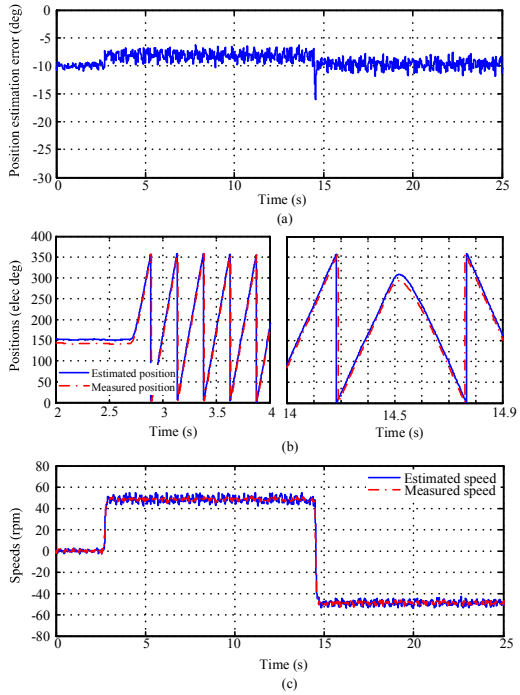

Fig. 16. Experimental results, speed step change with 40% rated torque, 50 rpm: (a) position estimation error; (b) position estimation at transients; (c) speed estimation.

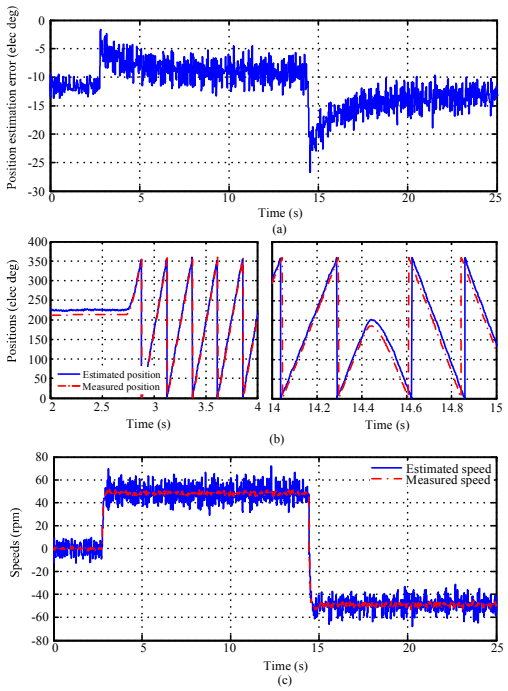

Fig. 18. Benchmark reference, speed and position estimation with pulsating voltage injection method with the same test shown in Fig. 16: (a) position estimation error; (b) position estimation at transients; (c) speed estimation.

shown in Fig. 18 (c) and Fig. 16 (c), both methods were tuned to have the same 10% to 90% rise time (practical bandwidth related). However, the 2% settling times of the speed step change from 0 rpm to 50 rpm and from 50 rpm to -50 rpm are 4.3 s and 5.6 s respectively in the benchmark reference. In the proposed method, the settling time for both speed transients are only 0.1 s and 0.15 s. The settling times of the proposed method are 40 times smaller than those of the pulsating voltage injection method. The comparison also shows that the proposed method has lower transient and steady state position estimation errors. The maximum transient error is -26° with pulsating voltage injection method and is -16° with the proposed method. The estimated speed ripple is smaller with the proposed method (10 rpm peak to peak) than that with the pulsating voltage injection method (30 rpm peak to peak), which is illustrated in Fig. 16 (c) and Fig. 18 (c). Hence, it can be concluded that the proposed method outperforms sinusoidal voltage injection based methods that use demodulation for speed and position sensing in the prototype IPM motor drive system.

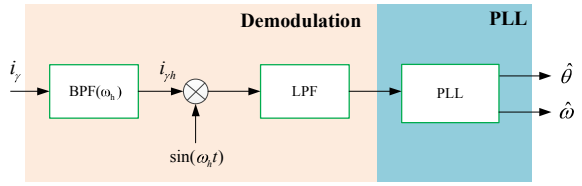

Fig. 17. Block diagram of the benchmark demodulation based position estimator [24]–[26].

In Fig. 19, the 40% rated torque was added on the shaft and the motor was tested with 100 rpm speed transients. In Fig. 16 and Fig. 19, the steady state position estimation error at 0 rpm, 50 rpm and 100 rpm with same 40% rated electromagnetic torque are -10°, -8.5° and -1.5°. Since the back-emf components become more significant as the speed increases, the position estimation error is reduced at higher speeds with the same torque applied on the shaft.

C. Torque Transients Performance

The speed and position estimation performance of the proposed method and the benchmark reference were also investigated with the torque transients tests. In Fig. 20, the motor was running constantly at 200 rpm. The electromagnetic torque changed from 40% rated torque to -40% rated torque. The similar tracking performance is observed in the current and speed transients in Fig. 20 (b) and (d). However, the longer settling time, the larger position estimation ripple, the larger steady state position estimation error and the larger estimated speed ripple are obtained with the benchmark reference method in Fig. 20 (a) and (d). With the position estimation errors in Fig. 20 (a), larger q axis current ripples are obtained with the benchmark reference method than the proposed method, as shown in Fig. 20 (c). The high current ripples will lead to higher torque ripples which degrades the motor performance.

In Fig. 21, the motor was running at 300 rpm. The electromagnetic torque changed from 76% rated torque to -76% rated torque. The torque change is reflected in the change of i_γ. The maximum transient position estimation error is within 15° electrical degree and the steady state estimation error is within 2.5°. Compared with Fig. 16 and Fig. 19, the transient and steady state position estimation errors are smaller with heavier torque. This is due to the increase of the back-emf

This article has been accepted for publication in a future issue of this journal, but has not been fully edited. Content may change prior to final publication. Citation information: DOI 10.1109/TPEL.2016.2621064, IEEE Transactions on Power Electronics

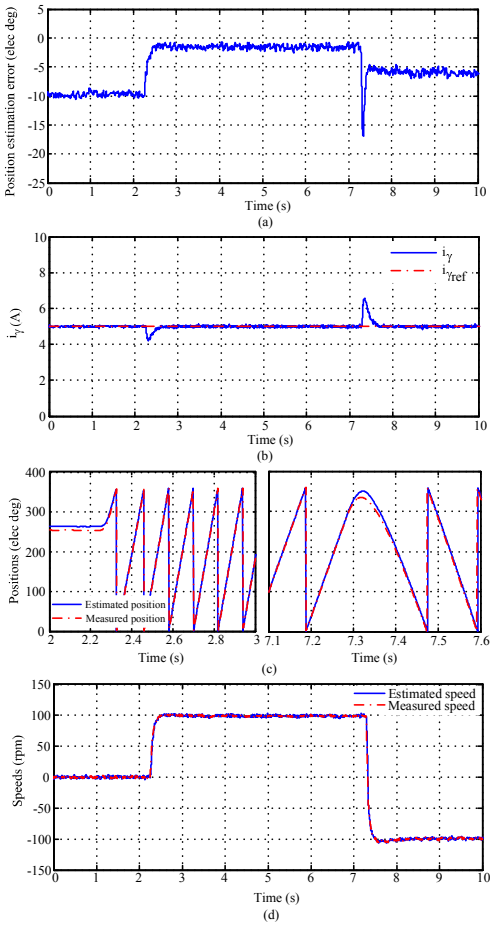

Fig. 19. Experimental results, speed step change with 40% rated torque, 100 rpm: (a) position estimation error; (b) current in γ axis; (c) position estimation at transients; (d) speed estimation.

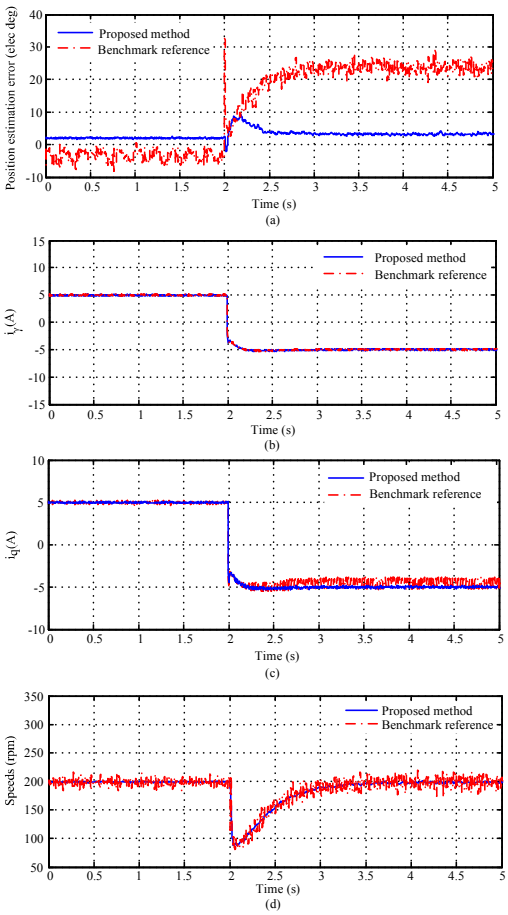

Fig. 20. Comparison between proposed method and benchmark reference, torque step change at constant speed, 200 rpm: (a) position estimation error; (b) current in γ axis; (c) current in q axis; (d) speed estimation.

which is proportional to the motor speed. The same test shown in Fig. 21 was also implemented with the pulsating voltage injection based method. However, the estimation failed due to the divergence of the estimator during the torque transients.

D. Wide Speed Range Operation

Fig. 22 illustrates the capability of sensorless operation at wide speed range. The motor speeds changed between different positive and negative values. The transitions between low speed (with injection and modified cost function (7)) and high speed (without injection and with original cost function (6)) are smooth. The steady state position estimation error is within $\pm 5^\circ$ electrical degree.

E. Parameter Sensitivity Analysis

In order to better evaluate the robustness of the proposed estimation method, the sensitivity of the motor parameters is analyzed with contour plots in Fig. 23 and experimental testing results in Fig. 24. In Fig. 23, the position estimation errors are analyzed with 50% resistance variation, 50% permanent magnet flux variation and 50% inductance variation (saliency ratio is kept constant) assuming the motor is running at 300 rpm with 40% rated torque. The position estimation errors under those parameter variations are 0°, 0° and 5.7° respectively. In the experimental tests shown in Fig. 24, the motor was running at 300 rpm and the electromagnetic torque changed from 40% rated torque to -40% rated torque. The position estimation errors due to 50% resistance variation, 50% permanent magnet flux variation and 50% inductance variation with 40% rated torque are 1.5°, 0.5° and 8.5°. Under the same test condition, the position estimation errors observed in experiment are larger than those in the theoretical contour plot analysis due to the measurement noise and model mismatch. Besides the 300 rpm and 40% rated torque test condition with 50% parameter variations, the results shown in Fig. 24 also illustrate the performance of the proposed method at torque transients, -40% rated torque condition and -50% parameter variations. From the results, it is clear that the position estimation errors during the torque transients are larger with $\pm 50\%$ parameter variations than the original values. Regarding the steady state estimation accuracy, the proposed estimation method is less affected by the resistance and permanent magnet flux variations. However, the steady state position estimation errors change by around 7° electrical degrees with $\pm 50\%$ inductance variations.

F. Computational Burden Analysis

The online optimization technique used in the real time implementation of the proposed method was introduced in

This article has been accepted for publication in a future issue of this journal, but has not been fully edited. Content may change prior to final publication. Citation information: DOI 10.1109/TPEL.2016.2621064, IEEE Transactions on Power Electronics

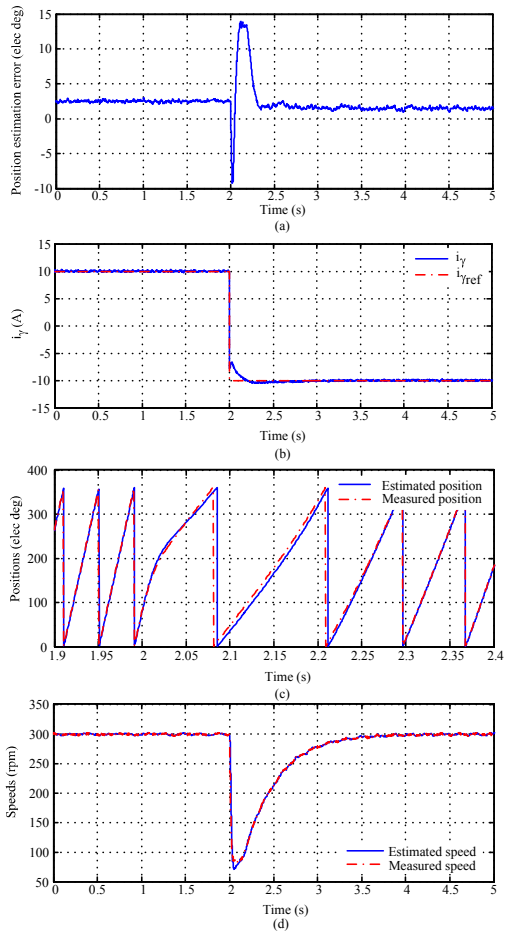

Fig. 21. Experimental results, torque step change at constant speed, 300 rpm: (a) position estimation error; (b) current in γ axis; (c) position estimation at transients; (d) speed estimation.

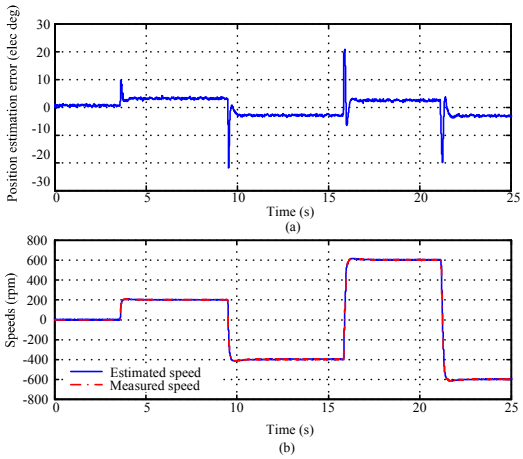

Fig. 22. Experimental results, wide speed range operation: (a) position estimation error; (b) speed estimation.

Section III. A certain number of iterations are both needed in search the optimal coefficient ξ and the minimum cost in a certain decent direction. The maximum iterations that the MicroAutoBox II can handle with 10 KHz sampling frequency is 18 iterations and the minimum iteration number is 1. The computational burden is reflected in the turnaround time (TAT) of the control system. The TATs of the proposed

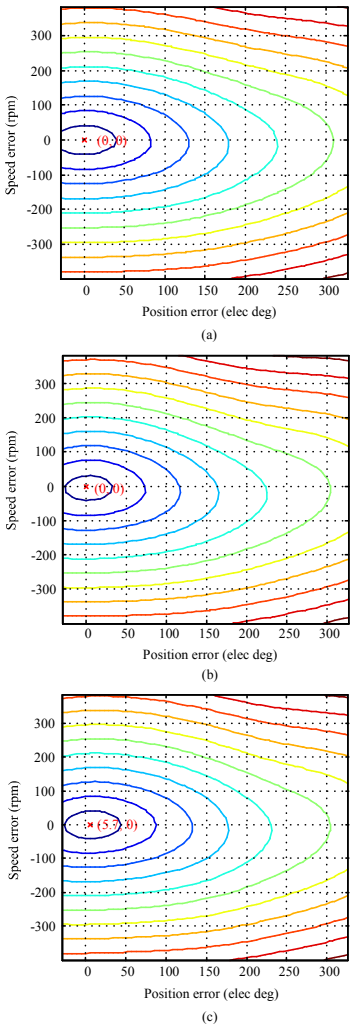

Fig. 23. Parameter sensitivity contour plot analysis at 300 rpm with 40% rated torque: (a) 50% resistance variation; (b) 50% permanent magnet flux variation; (c) 50% d-q axes inductances variation.

method with maximum and minimum iterations are 85 μs and 33 μs respectively. The TAT of the benchmark reference method is 29 μs which is close to the proposed method with minimum iteration. The estimation performances of the proposed method with maximum and minimum iterations and the benchmark reference method are compared in Fig. 25. The test conditions in Fig. 25 (a) and (b) are consistent with Fig. 19 and Fig. 20, which illustrate the speed and torque transients respectively. From the comparison of position estimation errors, it is concluded that the proposed method with minimum iteration has similar performance with maximum iterations. This performance similarity is due to the capability of executing the online optimization in the sampling frequency. Moreover, the TAT of the proposed method with minimum iteration is close to the benchmark reference but outperforms the benchmark reference method in dynamic response speed and steady state estimation accuracy.

G. Low Sampling Frequency Estimation Capability

Estimating speed and position with low sampling frequency is attractive for high power AC motor drives, which is challenging for the demodulation based position estimators at

This article has been accepted for publication in a future issue of this journal, but has not been fully edited. Content may change prior to final publication. Citation information: DOI 10.1109/TPEL.2016.2621064, IEEE Transactions on Power Electronics

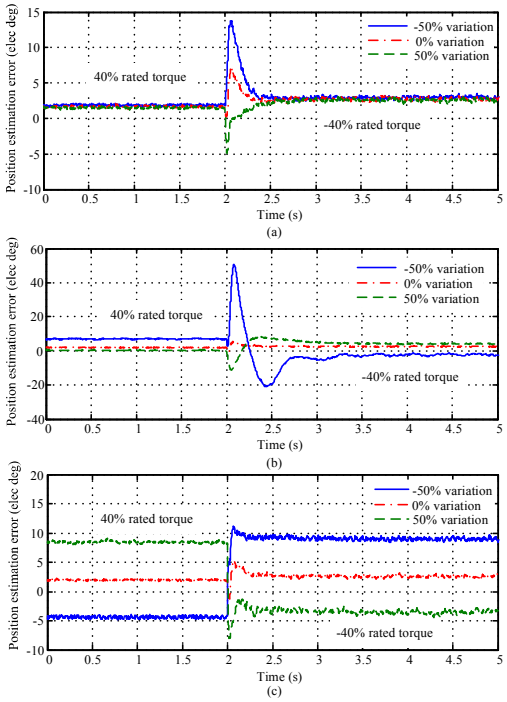

Fig. 24. Parameter sensitivity experimental test results: (a) $\pm 50\%$ resistance variation; (b) $\pm 50\%$ PM flux variation; (c) $\pm 50\%$ d-q axes inductances variation.

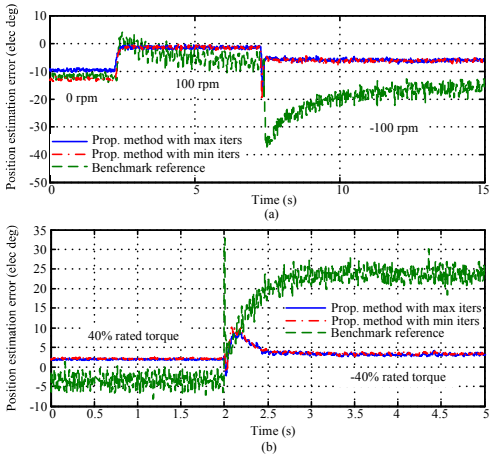

Fig. 25. Estimation performance validation with different iterations: (a) speed transients; (b) torque transients.

low speed. These estimators rely on the demodulation of the carrier frequency components that usually have much higher frequency than the fundamental frequency components. In the benchmark reference method, the frequency of the injected sinusoidal voltage is 500 Hz. If the sampling frequency is 10 KHz, the sinusoidal waveform can be sampled properly. However, if the sampling frequency is reduced to 2 KHz, there are only 4 samples in each sinusoidal period, which affects the estimation. The demodulation based method fails to extract speed and position information in the prototype motor drive system with 2 KHz sampling frequency while the proposed method is able to deliver the estimation.

Fig. 26 depicts the speed and position estimation results of the proposed method with 2 KHz sampling frequency. The testing condition is consistent with Fig. 16. From the

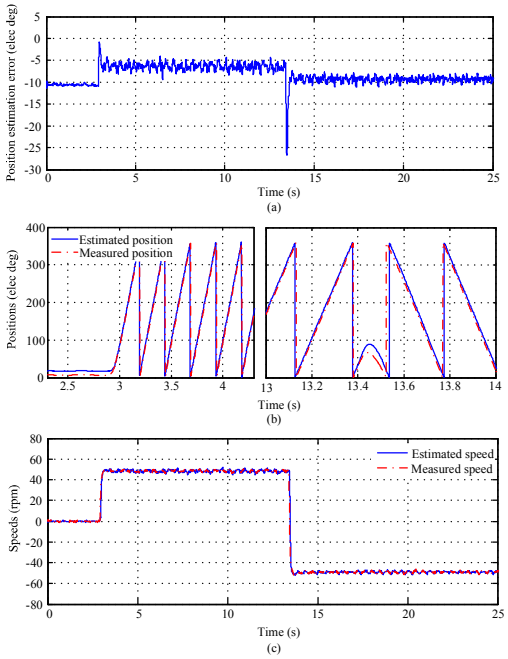

Fig. 26. Capability of delivering speed and position estimation with low sampling frequency.

comparison it is clear that the transient position estimation error increases with 2 KHz sampling frequency than that with 10 KHz sampling frequency, but the steady state estimation accuracies are very close in the two cases. The capability of performing speed and position estimation at low sampling frequency would make the proposed method promising in high power AC motor drives.

V. Conclusion

In this paper, a novel nonlinear optimization based speed and position estimation algorithm has been proposed. A cost function is defined based on the voltage equations in the stationary reference frame and the speed and position information can be obtained by minimizing the cost function. At low speed, the cost function is modified and extra high frequency voltage is injected to prevent the singularity at zero speed. Since the position estimator structure remains the same from standstill condition to high speed, a unified speed and position estimator is proposed for the IPM motor drives at wide speed range. The effectiveness of the cost functions has been validated with contour plot analysis and convexity analysis.

The real time implementation of the proposed estimator has been introduced and the feasibility of the proposed method has been validated with the prototype IPM motor drive system. The convergence range, performance with different speed and torque transients, computational burden and parameter sensitivity of the proposed method are presented in this paper. The experimental results demonstrate that the proposed method is capable of estimating the speed and position robustly with high accuracy and fast convergence.

At low speed and standstill conditions, the performances of the proposed method and the pulsating voltage injection based method have been compared under different test conditions. The proposed method outperforms with faster dynamic

response speed and lower transient and steady state estimation errors. Moreover, the proposed method is able to deliver speed and position estimation at 2 KHz sampling frequency, which is not realistic with the pulsating voltage injection based method.

ACKNOWLEDGMENT

This research was undertaken, in part, thanks to funding from the Canada Excellence Research Chairs Program.

REFERENCES

[1] Y. Sun, M. Preindl, S. Sirouspour, and A. Emadi, "Nonlinear modeling and design of initial position estimation and polarity detection of IPM drives," in *Conf. Rec. IEEE-IES (IECON'15) Annu. Meeting*, pp. 4059–4064, 2015.

[2] S. Morimoto, K. Kawamoto, M. Sanada, and Y. Takeda, "Sensorless control strategy for salient-pole PMSM based on extended EMF in rotating reference frame," *IEEE Trans. Ind. Appl.*, vol. 38, no. 4, pp. 1054–1061, 2002.

[3] Z. Chen, M. Tomita, S. Doki, and S. Okuma, "An extended electromotive force model for sensorless control of interior permanent-magnet synchronous motors," *IEEE Trans. Ind. Electron.*, vol. 50, no. 2, pp. 288–295, 2003.

[4] B. Nahid-Mobarakeh, F. Meibody-Tabar, and F.-M. Sargos, "Back EMF estimation-based sensorless control of PMSM: Robustness with respect to measurement errors and inverter irregularities," *IEEE Trans. Ind. Appl.*, vol. 43, no. 2, pp. 485–494, 2007.

[5] F. Genduso, R. Miceli, C. Rando, and G. R. Galluzzo, "Back EMF sensorless-control algorithm for high-dynamic performance PMSM," *IEEE Trans. Ind. Electron.*, vol. 57, no. 6, pp. 2092–2100, 2010.

[6] J. M. Liu and Z. Q. Zhu, "Improved sensorless control of permanent-magnet synchronous machine based on third-harmonic back EMF," *IEEE Trans. Ind. Appl.*, vol. 50, no. 3, pp. 1861–1870, 2014.

[7] S. Shinnaka, "New sensorless vector control using minimum-order flux state observer in a stationary reference frame for permanent-magnet synchronous motors," *IEEE Trans. Ind. Electron.*, vol. 53, no. 2, pp. 388–398, 2006.

[8] T. Chan, W. Wang, P. Borsje, Y. Wong, and S. Ho, "Sensorless permanent-magnet synchronous motor drive using a reduced-order rotor flux observer," *IET Electr. Power Appl.*, vol. 2, no. 2, pp. 88–98, 2008.

[9] M. Hasegawa and K. Matsui, "Position sensorless control for interior permanent magnet synchronous motor using adaptive flux observer with inductance identification," *IET Electr. Power Appl.*, vol. 3, no. 3, pp. 209–217, 2009.

[10] S. Chi, Z. Zhang, and L. Xu, "Sliding-mode sensorless control of direct-drive PM synchronous motors for washing machine applications," *IEEE Trans. Ind. Appl.*, vol. 45, no. 2, pp. 582–590, 2009.

[11] Y. Zhao, W. Qiao, and L. Wu, "An adaptive Quasi-Sliding-Mode rotor position observer-based sensorless control for interior permanent magnet synchronous machines," *IEEE Trans. Ind. Electron.*, vol. 28, no. 12, pp. 5618–5629, 2013.

[12] G. Wang, Z. Li, G. Zhang, Y. Yu, and D. Xiu, "Quadrature pll-based high-order sliding-mode observer for IPMSM sensorless control with online MTPA control strategy," *IEEE Trans. Energy Convers.*, vol. 28, no. 1, pp. 214–224, 2013.

[13] G. Wang, H. Zhan, G. Zhang, X. Gui, and D. Xiu, "Adaptive compensation method of position estimation harmonic error for EMF-based observer in sensorless IPMSM drives," *IEEE Trans. Power Electron.*, vol. 29, no. 6, pp. 3055–3064, 2014.

[14] Y. Zhao, W. Qiao, and L. Wu, "Dead-time effect analysis and compensation for a sliding-mode position observer-based sensorless IPMSM control system," *IEEE Trans. Ind. Appl.*, vol. 51, no. 3, pp. 2528–2535, 2015.

[15] Y. Zhao, Z. Zhang, W. Qiao, and L. Wu, "An extended flux Model-Based rotor position estimation for sensorless control of salient-pole permanent-magnet synchronous machines," *IEEE Trans. Power Electron.*, vol. 30, no. 8, pp. 4412–4422, 2015.

[16] S. Bolognani, R. Oboe, and M. Zigliotto, "Sensorless full-digital PMSM drive with EKF estimation of speed and rotor position," *IEEE Trans. Ind. Electron.*, vol. 46, no. 1, pp. 184–191, 1999.

[17] Y. Kim and Y. Kook, "High performance IPMSM drives without rotational position sensors using reduced-order EKF," *IEEE Trans. Energy Convers.*, vol. 14, no. 4, pp. 868–873, 1999.

[18] M. Boussak, "Implementation and experimental investigation of sensorless speed control with initial rotor position estimation for interior permanent magnet synchronous motor drive," *IEEE Trans. Power Electron.*, vol. 20, no. 6, pp. 1413–1422, 2005.

[19] H. Kim, K. Huh, R. D. Lorenz, and T. M. Jahns, "A novel method for initial rotor position estimation for IPM synchronous machine drives," *IEEE Trans. Ind. Appl.*, vol. 40, no. 5, pp. 1369–1378, 2004.

[20] Y. Jeong, R. D. Lorenz, T. M. Jahns, and S. Sul, "Initial rotor position estimation of an interior permanent-magne synchronous machine using carrier-frequency injection methods," *IEEE Trans. Ind. Appl.*, vol. 41, no. 1, pp. 38–45, 2005.

[21] S. Bolognani, S. Calligaro, R. Petrella, and M. Tursini, "Sensorless control of IPM motors in the low-speed range and at standstill by HF injection and DFT processing," *IEEE Trans. Ind. Appl.*, vol. 47, no. 1, pp. 96–104, 2011.

[22] S. Kim, J. Ha, and S. Sul, "PWM switching frequency signal injection sensorless method in IPMSM," *IEEE Trans. Ind. Appl.*, vol. 48, no. 5, pp. 1576–1587, 2012.

[23] T. Aihara, A. Toba, T. Yanase, A. Mashimo, and K. Endo, "Sensorless torque control of salient-pole synchronous motor at zero-speed operation," *IEEE Trans. Power Electron.*, vol. 14, no. 1, pp. 202–208, 1999.

[24] J. Jang, J. Ha, M. Ohto, K. Ide, and S. Sul, "Analysis of permanent-magnet machine for sensorless control based on high-frequency signal injection," *IEEE Trans. Ind. Appl.*, vol. 40, no. 6, pp. 1595–1604, 2004.

[25] G. Foo, S. Sayeef, and M. F. Rahman, "Low-speed and standstill operation of a sensorless direct torque and flux controlled IPM synchronous motor drive," *IEEE Trans. Energy Convers.*, vol. 25, no. 6, pp. 25–33, 2010.

[26] L. M. Gong and Z. Q. Zhu, "Robust initial rotor position estimation of permanent-magnet brushless AC machines with carrier-signal-injection-based sensorless control," *IEEE Trans. Ind. Appl.*, vol. 49, no. 6, pp. 2602–2609, 2013.

[27] S. Zaim, B. Nahid-Mobarakeh, and F. Meibody-Tabar, "Robust position sensorless control of nonsalient PMSM at standstill and low speed," *IEEE Trans. Emerg. Sel. Topics Power Electron.*, vol. 2, no. 3, pp. 640–650, 2014.

[28] Z. Huang, L. You, and Z. Wang, "Sensorless initial rotor position identification for non-salient permanent magnet synchronous motors based on dynamic reluctance difference," *IET Power Electron.*, vol. 7, no. 9, pp. 2336–2346, 2014.

[29] S. Yang, "Saliency-based position estimation of permanent-magnet synchronous machines using square-wave voltage injection with a single current sensor," *IEEE Trans. Ind. Appl.*, vol. 51, no. 2, pp. 1561–1571, 2015.

[30] T. Noguchi, K. Yamada, S. Kondo, and I. Takahashi, "Initial rotor position estimation method of sensorless PM synchronous motor with no sensitivity to armature resistance," *IEEE Trans. Ind. Electron.*, vol. 45, no. 1, pp. 118–125, 1998.

[31] J. M. Liu and Z. Q. Zhu, "Novel sensorless control strategy with injection of high-frequency pulsating carrier signal into stationary reference frame," *IEEE Trans. Ind. Appl.*, vol. 50, no. 4, pp. 2574–2583, 2014.

[32] M. Schroedl, "Sensorless control of AC machines at low speed and standstill based on the "INFORM" method," in *Conf. Rec. IEEE IAS Annu. Meeting*, vol. 1, pp. 270–277, 1996.

[33] V. Petrovic, A. M. Stankovic, and V. Blasko, "Position estimation in salient PM synchronous motors based on PWM excitation transients," *IEEE Trans. Ind. Appl.*, vol. 39, no. 3, pp. 835–843, 2003.

[34] C. Silva, G. M. Asher, and M. Sumner, "Hybrid rotor position observer for wide speed-range sensorless PM motor drives including zero speed," *IEEE Trans. Ind. Electron.*, vol. 53, no. 2, pp. 373–378, 2006.

[35] G. Bisheimer, M. Sonnaillon, C. DeAngelo, J. Solsona, and G. Garcia, "Full speed range permanent magnet synchronous motor control without mechanical sensors," *IET Electr. Power Appl.*, vol. 4, no. 1, pp. 35–44, 2010.

[36] G. Andreescu, C. I. Pitic, F. Blaabjerg, and I. Boldea, "Combined flux observer with signal injection enhancement for wide speed range sensorless direct torque control of IPMSM drives," *IEEE Trans. Energy Convers.*, vol. 23, no. 2, pp. 393–402, 2008.

[37] G. Wang, R. Yang, and D. Xu, "DSP-based control of sensorless IPMSM drives for wide-speed-range operation," *IEEE Trans. Ind. Electron.*, vol. 60, no. 2, pp. 720–727, 2013.

[38] Z. Ma, J. Gao, and R. Kennel, "FPGA implementation of a hybrid sensorless control of SMPMSM in the whole speed range," *IEEE Trans. Ind. Informat.*, vol. 9, no. 3, pp. 1253–1261, 2013.

[39] S. Bolognani, A. Faggion, E. Fornasiero, and L. Sgarbossa, "Full speed range sensorless IPM motor drives," in *Conf. Rec. International Conference on Electrical Machines*, pp. 2209–2215, 2012.

[40] M. Preindl, "Robust control invariant sets and lyapunov-based mpc for ipm synchronous motor drives," *IEEE Trans. Ind. Electron.*, vol. 63, no. 6, pp. 3925–3933, 2016.
[41] S. Boyd and L. Vandenberghe, *Convex Optimization*. New York, NY: Cambridge University Press, 2004. ISBN: 0-521-83378-7.
[42] B. Nahid-Mobarakeh, F. Meibody-Tabar, and F.-M. Sargos, "Mechanical sensorless control of PMSM with online estimation of stator resistance," *IEEE Trans. Ind. Appl.*, vol. 40, no. 2, pp. 457–471, 2004.
[43] E. Al-nabi, B. Wu, N. R. Zargari, and V. Sood, "Sensorless control of CSC-Fed IPM machine for zero- and Low-Speed operation using pulsating hfi method," *IEEE Trans. Ind. Electron.*, vol. 60, no. 5, pp. 1711–1723, 2013.
[44] M. Preindl and S. Bolognani, "Model predictive direct speed control with finite control set of pmsm drive systems," *IEEE Trans. Power Electron.*, vol. 28, no. 2, pp. 1007–1015, 2012.
[45] P. Guglielmi, M. Pastorelli, and A. Vagati, "Cross-saturation effects in ipm motors and related impact on sensorless control," *IEEE Trans. Ind. Appl.*, vol. 42, no. 6, pp. 1516–1522, 2006.
[46] Y. Li, Z. Zhu, D. Howe, C. M. Bingham, and D. A. Stone, "Improved rotor-position estimation by signal injection in brushless ac motors, accounting for cross-coupling magnetic saturation," *IEEE Trans. Ind. Appl.*, vol. 45, no. 5, pp. 1843–1850, 2009.

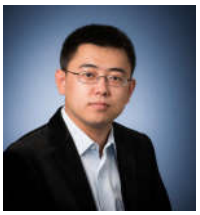

Yingguang Sun (S'15) received the B.S. degree in Electrical Engineering from Hebei University of Technology, Tianjin, China, in 2011 and the M.S. degree in Electrical Engineering from Illinois Institute of Technology (IIT), Chicago, IL, USA, in 2013. In September 2013, he joined the McMaster Institute for Automotive Research and Technology (MacAUTO), McMaster University, Hamilton, ON, Canada, where he is currently working toward the Ph.D. degree in Electrical Engineering.

From September 2012 to June 2013, he served as a Research Assistant with Electric Drives and Energy Conversion Laboratory in IIT, Chicago, IL, USA. Currently, he is working as a Research Assistant for the Canada Excellence Research Chair in Hybrid Powertrain Program, Hamilton, ON, Canada. He obtained the best presentation prize in IECON 2015 at Yokohama, Japan. His main research areas include advanced control methods for electric machine drives and power electronics applications in electrified transportation systems.

Matthias Preindl (S'12-M'15) is an Assistant Professor in the Department of Electrical Engineering, Columbia University in the City of New York, USA. He received the PhD degree in Energy Engineering from the Doctoral School of Industrial Engineering at University of Padua, Italy (2014), the MSc degree in Electrical Engineering and Information Technology from ETH Zurich, Switzerland (2010), and the BSc degree in Electrical Engineering (summa cum laude) form University of Padua, Italy (2008).

M. Preindl was a Sessional Professor in the Department of Electrical and Computer Engineering (2015) and a Post Doctoral Research Associate at the McMaster Institute for Automotive Research and Technology (2014-2015), both at McMaster University, Canada. He was a visiting scholar at University of California, Berkeley, USA (2013), a visiting student at Aalborg University, Denmark (2009), and a trainee at the National Research Council (CNR), Italy (2008). M. Preindl worked in industry as a R&D engineer at Leitwind AG, Italy (2010-2012).

M. Preindl founded and leads the Motor Drives and Power Electronics Laboratory (MPLab) at Columbia University. He obtained several honors including best presentation awards, merit-based fellow and scholarships, and a price for outstanding achievements during his studies. His primary research interests are the design and control of power electronic and motor drive systems with applications in electrified transportation systems, renewable-energy power plants, and smart grids.

Shahin Sirouspour (S'00-M'04) received the B.Sc. and M.Sc. degrees in electrical engineering from Sharif University of Technology, Tehran, Iran, in 1995 and 1997, respectively, and the Ph.D. degree in electrical engineering from the University of British Columbia, Vancouver, BC, Canada, in 2003. He then joined McMaster University, Hamilton, ON, Canada, where he is currently a Professor in the Department of Electrical and Computer Engineering. His research interests include aerial robotics, teleoperation control, haptics, medical robotics, and optimization-based energy management and control in smart grid environment. He was on research leave at MDA Space Missions (Brampton, Ontario, Canada) during the period July 2010-June 2011. Dr. Sirouspour received the McMaster President's Award of Excellence in Graduate Supervision in 2008.

Ali Emadi (S'98-M'00-SM'03-F'13) received the B.S. and M.S. degrees in electrical engineering with highest distinction from Sharif University of Technology, Tehran, Iran, in 1995 and 1997, respectively, and the Ph.D. degree in electrical engineering from Texas A&M University, College Station, TX, USA, in 2000. He is the Canada Excellence Research Chair in Hybrid Powertrain at McMaster University in Hamilton, Ontario, Canada. Before joining McMaster University, Dr. Emadi was the Harris Perlstein Endowed Chair Professor of Engineering and Director of the Electric Power and Power Electronics Center and Grainger Laboratories at Illinois Institute of Technology (IIT) in Chicago, Illinois, USA, where he established research and teaching facilities as well as courses in power electronics, motor drives, and vehicular power systems. He was the Founder, Chairman, and President of Hybrid Electric Vehicle Technologies, Inc. (HEVT) a university spin-off company of IIT. Dr. Emadi has been the recipient of numerous awards and recognitions. He was the advisor for the Formula Hybrid Teams at IIT and McMaster University, which won the GM Best Engineered Hybrid System Award at the 2010, 2013, and 2015 competitions. He is the principal author/coauthor of over 350 journal and conference papers as well as several books including Vehicular Electric Power Systems (2003), Energy Efficient Electric Motors (2004), Uninterruptible Power Supplies and Active Filters (2004), Modern Electric, Hybrid Electric, and Fuel Cell Vehicles (2nd ed, 2009), and Integrated Power Electronic Converters and Digital Control (2009). He is also the editor of the Handbook of Automotive Power Electronics and Motor Drives (2005) and Advanced Electric Drive Vehicles (2014). Dr. Emadi was the Inaugural General Chair of the 2012 IEEE Transportation Electrification Conference and Expo (ITEC) and has chaired several IEEE and SAE conferences in the areas of vehicle power and propulsion. He is the founding Editor-in-Chief of the IEEE Transactions on Transportation Electrification.